Probing the Majorana nature of TeV-scale radiative seesaw models at the ILC

Mayumi Aoki[1] and Shinya Kanemura[2*]

1- Institute for Theoretical Physics, Kanazawa University, Kanazawa 920-1192, Japan

2- Department of Physics, University of Toyama, Toyama 930-8555, Japan

Two important features of TeV-scale radiative seesaw models, in which tiny neutrino masses are generated at the quantum level, are an extended scalar (Higgs) sector and the Majorana nature. We study phenomenological aspects of these models at the ILC. It is found that the Majorana nature of the models can be tested directly via the electron-positron and electron-electron collision experiments.

1 Introduction

Current neutrino data give clear evidence for physics beyond the standard model (SM), indicating that neutrinos have tiny masses of the 0.1 eV scale. Such tiny masses may be generated from dimension-five effective operators $\frac{c_{ij}}{2\Lambda}\overline{\nu^c}^i_L \nu^j_L \phi^0 \phi^0$, where Λ is a mass scale, c_{ij} are dimensionless coefficients, and ϕ^0 is the Higgs boson. The neutrino mass matrix can then be given by $M_\nu^{ij} = c_{ij}\langle\phi^0\rangle^2/\Lambda$. As the vacuum expectation value (VEV) $\langle\phi^0\rangle$ of the Higgs boson is $\mathcal{O}(100)$ GeV, the observed tiny neutrino masses are realized when $(c_{ij}/\Lambda) \sim \mathcal{O}(10^{-14})$ GeV^{-1}. How can we naturally explain such a small number? In the tree-level seesaw scenario, the Majorana masses of right-handed neutrinos ($= \Lambda$) have to be set much higher than the electroweak scale [1].

Quantum generation of neutrino masses can be an alternative to obtain $(c_{ij}/\Lambda) \sim \mathcal{O}(10^{-14})$ GeV^{-1}. Thanks to the loop suppression factor, Λ in these models can be lower as compared to that in the tree-level seesaw models. Consequently, the tiny neutrino masses would be explained in a natural way only by the TeV-scale dynamics. The original model along this line was proposed by Zee [2], and some variations were considered [3, 4, 5, 6, 7], where neutrino masses are induced at the one-, two- or three-loop level. It must be charming that they are directly testable at the LHC and the ILC.

A general feature in radiative seesaw models is the extended Higgs sector. Discovery of extra Higgs bosons and detailed measurements of their properties at future collider experiments can give partial evidence for the models. Previous works on phenomenology in radiative seesaw models[8, 9, 10] mainly discuss the constraint on the flavor structure and collider physics for the Higgs sector [11, 12, 13, 14, 15]. Next, the Majorana nature is another common feature. To induce tiny Majorana masses for neutrinos, we need lepton number violating interactions in the Higgs sector [2, 4] or right-handed neutrinos with TeV-scale Majorana masses [5, 6, 7]. When the future data would indicate an extended Higgs sector predicted by a specific radiative seesaw model, direct detection of the Majorana property at colliders must be a fatal probe to identify the model.

In this talk, we discuss phenomenology of TeV-scale radiative seesaw models, in particular a possibility of detecting the Majorana nature at collider experiments[16]. We here discuss three typical radiative seesaw models as reference models; the model by Zee and Babu [4], that by Ma [6], and that in Ref. [7].

*Speaker

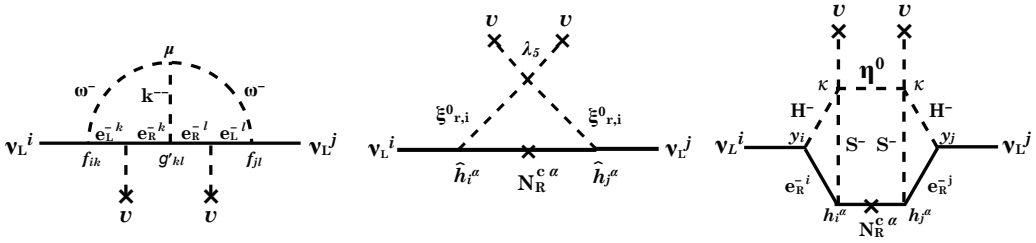

Figure 1: Feynman diagrams for neutrino masses in the model by Zee-Babu [4] (left), that by Ma [6] (center) and that in Ref. [7] (right).

2 Radiative seesaw models

The Zee-Babu model

In the model proposed in Ref. [4] (we refer to as the Zee-Babu model), in addition to singly-charged singlet scalar bosons $\omega^{\pm}$, doubly-charged singlet scalar fields $k^{\pm\pm}$ are introduced, both of which carry the lepton number of two unit. The neutrino mass matrix is generated at the two-loop level via the diagram in Fig. 1 (left). The universal scale of neutrino masses is determined by the two-loop suppression factor $1/(16\pi^2)^2$ and the lepton number violating parameter μ. The charged lepton Yukawa coupling constants y_{ℓ_i} ($y_e \ll y_\mu \ll y_\tau \lesssim 10^{-2}$) give an additional suppression factor. Thus, any of f_{ij} or g_{ij} in Fig. 1 (left) can be of $\mathcal{O}(1)$ when m_ω and m_k are at the TeV scale. The flavor structure of the mass matrix is determined by the combination of the coupling constants f_{ij} and $y_i g_{ij} y_j$. The flavor off-diagonal coupling constants f_{ij} and g_{ij} induce lepton flavor violation (LFV).

In the scenario with hierarchical neutrino masses, f_{ij} satisfy $f_{e\mu} \simeq f_{e\tau} \simeq f_{\mu\tau}/2$. The typical relative magnitudes among the coupling constants g_{ij} can be $g_{\mu\mu} : g_{\mu\tau} : g_{\tau\tau} \simeq 1 : m_\mu/m_\tau : (m_\mu/m_\tau)^2$. For $g_{\mu\mu} \simeq 1$, the neutrino data and the LFV data give the constraints such as $m_k \gtrsim 770$ GeV and $m_\omega \gtrsim 160$ GeV [9]. On the other hand, the constraints on the couplings and masses are more stringent for the inverted neutrino mass hierarchy. The current data then gives $m_\omega \simeq 825$ GeV for $g_{\mu\mu} \simeq 1$ [9]. One of the notable things in this case is the lower bound on $\sin^2 2\theta_{13}$, which is predicted as around 0.002 [8].

The Ma model

The model in Ref. [6], which we here refer to as the Ma model, is the simplest radiative seesaw model with right-handed neutrinos N_R^α, in which the discrete Z_2 symmetry is introduced and its odd quantum number is assigned to N_R^α. The Higgs sector is composed of two Higgs doublet fields, one of which (Ξ) is Z_2 odd. As long as the Z_2 symmetry is exact, the neutral components of Ξ do not receive VEVs. We have one SM-like Higgs boson h, and four physical Z_2-odd scalar states; ξ_r^0 (CP-even), ξ_i^0 (CP-odd) and $\xi^\pm$ as physical scalar states. This Z_2 odd Higgs doublet is sometimes called as the inert Higgs doublet [11] or the dark scalar doublet [12]. The LEP II limits are studied in this model in Ref. [17].

The neutrino masses are generated at the one loop level via the diagram depicted in Fig. 1 (center), in which Z_2 odd particles, ξ^0 and N_R^α, are in the loop. The universal scale for neutrino masses is determined by the one-loop suppression factor $1/(16\pi^2)$, the scalar coupling λ_5 and the mass $M_{N_R^\alpha}$ of the right-handed neutrinos.

In this model, there are two scenarios with respect to the DM candidate; i.e., the lightest right-handed neutrino N_R^1 or the lightest Z_2-odd neutral field (ξ_r^0 or ξ_i^0). For both cases, there are parameter regions where the neutrino data are adjustable without contradicting other phenomenological constraints [18]. In this talk, we consider the case where the dark doublet component ξ_r^0 is the DM candidate. If the mass of the DM is around 50 GeV, the mass difference between ξ_r^0 and ξ_i^0 is given by about 10 GeV when $\lambda_5 \sim 10^{-2}$. In this case, $\hat{h}_i^\alpha \sim 10^{-5}$ $(i = e, \mu, \tau)$ are required to satisfy the neutrino data. The relic abundance of such DM is consistent with the WMAP data [13].

The AKS model

In the model in Ref. [7], which we here refer to as the AKS model, it is intended that not only the tiny neutrino masses and DM but also baryon asymmetry of Universe are explained at the TeV scale. In addition to the TeV-scale right-handed neutrinos N_R^α $(\alpha = 1, 2)$, the Higgs sector is composed of Z_2-even two Higgs doublets Φ_i $(i = 1, 2)$, where the physical component fields are H (CP-even), A (CP-odd), $H^\pm$ and h (CP-even), and Z_2-odd charged singlets $S^\pm$ and a Z_2-odd neutral real singlet η^0. The neutrino mass matrix is generated at the three-loop level via the diagram in Fig. 1 (right). The mass matrix has the three loop factor $1/(16\pi^2)^3$ with additional suppression by the charged lepton Yukawa couplings y_i. The electron associated couplings $h_e^{1,2}$ and the scalar coupling κ are of $\mathcal{O}(1)$ for $m_{N_R}^{1,2} \sim \mathcal{O}(1)$ TeV. The Yukawa coupling constants h_i^α are hierarchical as $h_e^{1,2} (\simeq \mathcal{O}(1)) \gg h_\mu^{1,2} \gg h_\tau^{1,2}$.

The parameter sets which satisfy the current data from neutrino oscillation, LFV, relic abundances of DM and the condition for strongly first order electroweak phase transition are studied in Ref. [7]. To reproduce the neutrino data, the mass of $H^\pm$ should be 100 - 200 GeV. This is an important prediction of the model. In order to avoid the constraint from $b \to s\gamma$, the Yukawa interaction for the doublet fields takes the form of so-called Type-X [14] where only one of the doublets couples to leptons and the rest does to quarks[19]. The physics of the Type-X two Higgs doublet model (THDM) shows many distinctive features from the other type of extended Higgs sectors. For example, H and A decay mainly into $\tau^+\tau^-$ when $\tan\beta \gtrsim 3$ and $\sin(\beta - \alpha) \simeq 1$ [14]. There are basically two DM candidates, η^0 and N_R^α. We here consider the case where η^0 is the DM[7]. Some characteristics of η^0 are discussed in Refs. [20]. The coupling constant of S^+S^-h is required to be of $\mathcal{O}(1)$ for strongly first order phase transition, whose indirect effect appears in the quantum correction to the hhh coupling constant as a large deviation from the SM prediction [7]. As long as kinematically allowed, $S^\pm$ decays via $S^\pm \to H^\pm\eta^0$ by 100%.

3 Phenomenology in radiative seesaw models at the LHC

The existence of the extra Higgs bosons such as charged scalar bosons, which are a common feature of radiative seesaw models, can be tested at the LHC. Details of the properties of such extra Higgs bosons are strongly model dependent, so that we can distinguish models via detailed measurements of extra Higgs bosons. In addition, as the (SM-like) Higgs boson h is expected to be detected, its mass and decay properties are thoroughly measured [21]. The radiative seesaw models with a DM candidate can also be indirectly tested via the invisible decay of h as long as its branching ratio is more than about 25% for $m_h = 120$ GeV with $\mathcal{L} = 30$ fb^{-1} [22]. The phenomenological analyses at the LHC in each model are in the literature [8, 9, 10, 12, 14, 15].

At the LHC, via the physics of extra scalar bosons such as (singly and/or doubly) charged

Higgs bosons and CP-even Higgs bosons, the structure of the extended Higgs sector can be clarified to some extent. In addition, the invisible decay of the SM-like Higgs boson and the mass spectrum of the extra Higgs bosons would give important indication for a possibility to a radiative seesaw scenario. However, although they would be a strong indication of radiative seesaw models, one cannot conclude that such Higgs sector is of the radiative seesaw models. In order to further explore the possibility to such models, we have to explore the other common feature of radiative seesaw models, such as the Majorana nature. In the next section, we discuss a possibility of testing the Majorana nature at ILC experiments.

4 Phenomenology in radiative seesaw models at the ILC

At the ILC, properties of the Higgs sector can be measured with much better accuracy than at the LHC, so that we would be able to reconstruct the Higgs potential in any extended Higgs sector if kinematically accessible. Invisible decays of the Higgs boson can also be tested when the branching ratio $B(h \to invisible)$ is larger than a few % [23]. Furthermore, the Majorana nature in radiative seesaw models; *i.e.,* the existence of TeV scale right-handed Majorana neutrinos or that of LFV interaction, would also be tested.

4.1 Electron-positron collisions

In the pair production of charged scalar bosons at the e^+e^- collision, which appear in the radiative seesaw models ($\omega^+\omega^-$ in the Zee-Babu model, $\xi^+\xi^-$ in the Ma model, and S^+S^- (and H^+H^-) in the AKS model), there are diagrams of the t-channel exchange of left-handed neutrinos or right-handed neutrinos in addition to the usual Drell-Yan type s-channel diagrams. The contribution of these t-channel diagrams is one of the discriminative features of radiative seesaw models, and no such contribution enters into the other extended Higgs models such as the THDM. These t-channel effects show specific dependences on the center-of-mass energy $\sqrt{s}$ in proportion to $\log s$ in the production cross section, and enhances the production rates of the signal events for higher values of $\sqrt{s}$. The final states of produced charged scalar boson pairs are quite model dependent but with missing energy;

$$e^+e^- \to \omega^+\omega^- \to \ell_L^+\ell_L^-\underline{\overline{\nu}_L\nu_L}\,, \qquad \text{[The Zee−Babu model]}$$
$$e^+e^- \to \xi^+\xi^- \to W^{+(*)}W^{-(*)}\xi_r^0\xi_r^0 \to jjjj(jj\ell_L\underline{\nu_L})\underline{\xi_r^0\xi_r^0}\,, \qquad \text{[The Ma model]}$$
$$e^+e^- \to S^+S^- \to H^+H^-\eta^0\eta^0 \to \tau_R^+\tau_R^-\underline{\overline{\nu}_L\nu_L\eta^0\eta^0}\,, \qquad \text{[The AKS model]}$$

where underlined parts in the final states are observed as missing energy.

<u>*The Ma model*</u>: The coupling constants $\hat{h}_e^\alpha$ ($\alpha = 1, 2$) are strongly constrained from neutrino data and LFV data. As a typical choice of parameters, we consider $m_{\xi_r} = 50$ GeV, $m_{\xi_i} = 60$ GeV, $m_{\xi^\pm} \sim 100$ GeV, $m_{N_R^1} = m_{N_R^2} = 3$ TeV, $\lambda_5 = -1.8\times10^{-2}$, $\hat{h}_e^\alpha, \hat{h}_\mu^\alpha, \hat{h}_\tau^\alpha \sim 10^{-5}$, in which the normal neutrino mass hierarchy is realized. Because $\hat{h}_e^\alpha$ are very small for a TeV scale $m_{N_R^\alpha}$, the contribution of the t-channel diagrams to the signal $e^+e^- \to \xi^+\xi^-$ is much smaller than that from Drell-Yan type diagrams. For most of the possible values of $\hat{h}_\ell^\alpha$ and $m_{N_R^\alpha}$ which satisfy the LFV and the neutrino data, the contribution of the t-channel diagrams is negligible. The production cross section of a charged Higgs pair $\xi^+\xi^-$ is therefore similar

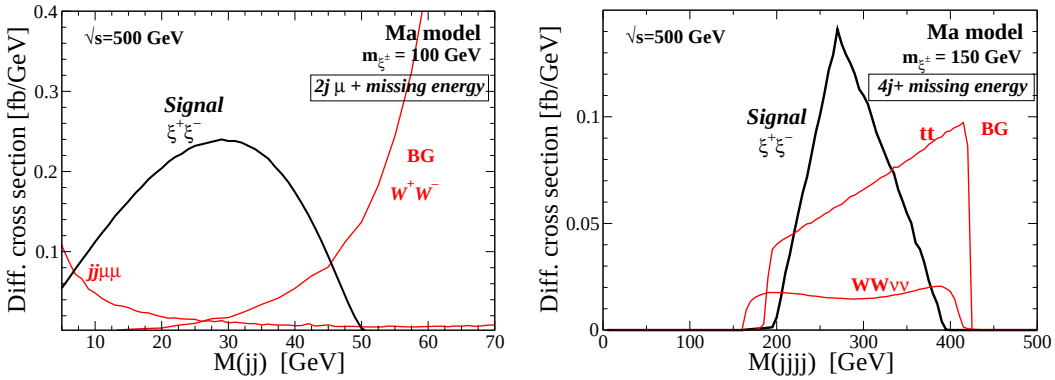

Figure 2: The jets invariant mass distributions of the production rates of the signal in the Ma model at $\sqrt{s} = 500$ GeV. *left* : The di-jet invariant mass $M(jj)$ distribution of the signal $e^+e^- \to \xi^+\xi^- \to jj\mu\nu\xi_r^0\xi_r^0$ for $m_{\xi^\pm} = 100$ GeV. *right* : $M(jjjj)$ distribution of $e^+e^- \to \xi^+\xi^- \to W^+W^-\xi_r^0\xi_r^0 \to jjjj\xi_r^0$ for $m_{\xi^\pm} = 150$ GeV. In addition to the rate from the signal process, those for main backgrounds are also shown.

to that in the usual THDM: about 92 (10) fb for $m_{\xi^\pm} = 100$ (150) GeV at $\sqrt{s} = 500$ GeV. The produced $\xi^\pm$ decay into $W^{\pm(*)}\xi_{r,i}^0$.

In Fig. 2 (*left*), we show the invariant mass distribution of the di-jet jj of the production cross section of the signal, $e^+e^- \to \xi^+\xi^- \to W^{+*}W^{-*}\xi_r^0\xi_r^0 \to jj\mu\nu\xi_r^0\xi_r^0$ for $m_{\xi^\pm} = 100$ GeV. The main backgrounds come from WW. The $jj\mu\mu$ events from ZZ, $\gamma\gamma$, and $Z\gamma$ can also be the backgrounds. A factor of 0.1 is multiplied to the rate of the $jj\mu\mu$ backgrounds for the miss-identification probability of a muon. The signal is significant around $M(jj) \sim$30 GeV. The invariant mass cut (such as 15 GeV$< M(jj) <$ 40 GeV) is effective to reduce the backgrounds. For the numerical evaluation, we have used a package CalcHEP 2.5.4 [24].

For $m_{\xi^\pm} > m_W + m_{\xi_r}$, on the other hand, the signal $W^+W^-\xi_r^0\xi_r^0$ can be measured by detecting the events of four jets with a missing energy. The main background comes from $W^+W^-\nu\nu$ and $t\bar{t}$. By the invariant mass cuts of two-jet pairs at the W boson mass, the biggest background from WW can be eliminated. In Fig. 2 (*right*), we show the invariant mass distribution of $jjjj$ of the production cross sections of the signal and the backgrounds without any cut. A factor of 0.1 is multiplied to the rate of tt background, by which the probability of the lepton from a W that escapes from detection is approximately taken into account. The signal is already significant. The invariant mass cut ($M(jjjj) < 300$ GeV) gives an improvement for the signal/background ratio.

The AKS model: We take a typical successful scenario for the neutrino data with the the normal mass hierarchy, the LFV data and the DM data as well as the condition for strongly first order phase transition [7]; $m_\eta = 50$ GeV, $m_{H^\pm} = 100$ GeV, $m_{S^\pm} = 400$ GeV, $m_{N_R^1} = m_{N_R^2} = 3$ TeV, $\kappa \sim \mathcal{O}(1)$, $h_e^1 = h_e^2 = 2 \gg h_\mu^1$, $h_\mu^2 \gg h_\tau^1$, h_τ^2, $\sin(\beta - \alpha) = 1$, $\tan\beta = 10$. Because $h_e^{1,2} \sim \mathcal{O}(1)$, the contribution from the t-channel N_R^α exchange diagrams to the production cross section of S^+S^- dominate that from the Drell-Yan diagrams [7]. The cross section is about 87 fb for $m_{S^\pm} = 400$ GeV at $\sqrt{s} = 1$ TeV. As the decay branching ratio of

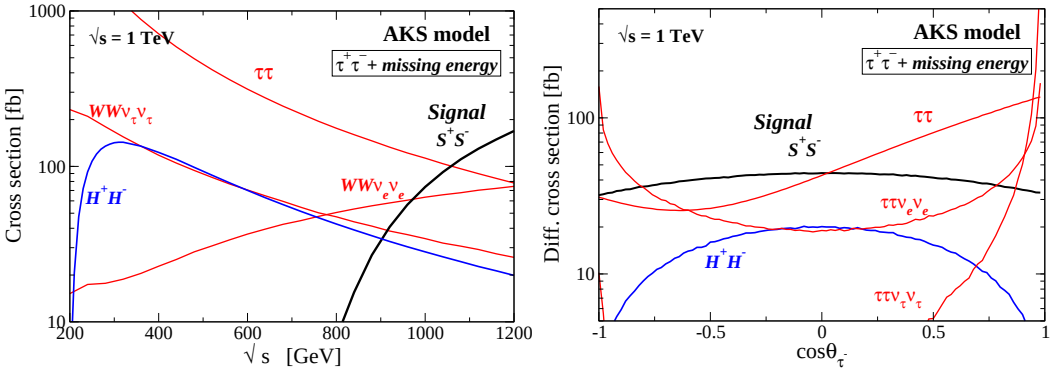

Figure 3: *left* : The cross sections of the signal, $e^+e^- \to S^+S^- \to \tau^+\tau^-$ (+ missing energy), in the AKS model as a function of the collision energy $\sqrt{s}$. *right* : The differential cross section of the signal for $\sqrt{s} = 1$ TeV as a function of the angle of the direction of the outgoing τ^- and the beam axis of incident electrons. In addition to the rate from the signal, those from backgrounds such as $\tau^+\tau^-$, $\tau^+\tau^-\overline{\nu}\nu$ and H^+H^- are also shown.

$S^\pm \to H^\pm\eta^0$ is 100% and that of $H^\pm \to \tau^\pm\nu$ is also almost 100% because of the Type-X THDM interaction for $\tan\beta = 10$, the final state of the signal is $\tau^+\tau^-\overline{\nu}\nu\eta^0\eta^0$ with almost the same rate as the parent S^+S^- production. The main SM backgrounds are $\tau^+\tau^-$ and $\tau^+\tau^-\overline{\nu}\nu$. The pair production of the doublet like charged Higgs boson H^+H^- can also be the background. As the signal rate dominantly comes from the t-channel diagram, it becomes larger for larger $\sqrt{s}$, while the main backgrounds except for $\tau\tau\nu_e\nu_e$ are smaller because they are dominantly s-channel processes (Fig. 3 (*left*)). At $\sqrt{s} = 1$ TeV, the rate of the signal without cut is already large enough as compared to those of the backgrounds. It is expected that making appropriate kinematic cuts will improve the signal background ratio to a considerable extent. The $\sqrt{s}$ scan will help us to confirm that the signal rate comes from the t-channel diagrams. Fig. 3 (*right*) shows the differential cross section of the signal at $\sqrt{s} = 1$ TeV as a function of $\cos\theta_{\tau^-}$, where θ_{τ^-} is the angle between the direction of the outgoing τ^- and the beam axis of incident electrons. The distribution of the background from $\tau\tau$ is asymmetric, so that the angle cut for larger $\cos\theta_{\tau^-}$ reduces the backgrounds.

4.2 Electron-electron collisions

The ILC has a further advantage to test radiative seesaw models via the experiment at the e^-e^- collision option, where dimension five operator of $e^-e^-\phi^+\phi^+$, which is the sub-diagram of the loop diagrams for neutrino mass matrix. This direct test of the dimension five operator is essential to identify the radiative seesaw models.

The Majorana nature in the Zee-Babu model is in the lepton number violating coupling constant μ of $k^{++}\omega^-\omega^-$, which generates the dimension five operator of $e^-e^-\omega^+\omega^+$ at the tree level via the s-channel k^{--} exchange. The cross section of $e^-e^- \to \omega^-\omega^-$ is given by

$$\sigma(e^-e^- \to \omega^-\omega^-) = \frac{1}{8\pi}\sqrt{1-\frac{4m_\omega^2}{s}}\,\frac{\mu^2 g_{ee}^2}{(s-m_k^2)^2+m_k^2\Gamma_k^2}, \qquad (1)$$

where Γ_k is the total width of $k^{\pm\pm}$. In the Ma model and the AKS model the operator

comes from the t-channel N_R^α exchange diagram. The cross section is evaluated as

$$\sigma(e^-e^- \to \phi^-\phi^-) = \int_{t_{\rm min}}^{t_{\rm max}} dt \frac{1}{128\pi s} \left| \sum_{\alpha=1}^{n} (|c^\alpha|^2 m_{N_R^\alpha}) \left(\frac{1}{t - m_{N_R^\alpha}^2} + \frac{1}{u - m_{N_R^\alpha}^2} \right) \right|^2 , \qquad (2)$$

where n is the number of generation of right-handed neutrinos, ϕ^- represents the Z_2-odd charged scalar boson ξ^- in the Ma model and S^- in the AKS model. The constants c^α represent $\hat{h}_e^\alpha$ or h_e^α in the Ma model or the AKS model, respectively. Due to the Majorana nature of the t-channel diagram, we obtain much larger cross section in the e^-e^- collision than in the e^+e^- collision in each model.

The mass matrix of left-handed neutrinos is generated at the one, two and three loop levels in the Ma model, the Zee-Babu model and the AKS model, respectively. Therefore, the coupling constants can be basically hierarchical among the models, so are the cross sections. For the typical scenarios in these models, the cross sections are shown in Fig. 4. The rate of $\omega^-\omega^-$ in the Zee-Babu model can be larger than several times 100 fb for 800 GeV $\lesssim \sqrt{s} \lesssim$ 1.5 TeV, where $m_\kappa = 1200$ GeV, $\mu = 800$ GeV and $g_{ee} = 0.17$ are asuumed, and Γ_k is computed as about 168 GeV in our scenario (see [16]). It becomes maximal (several times pb) at $\sqrt{s} \sim m_k$, and above that asymptotically reduces by $1/s$. The maximal value of the cross section is sensitive to the value of g_{ee} and μ. The signal should be like-sign dilepton with a missing energy. On the other hand, in the Ma model, production cross sections of $e^-e^- \to \xi^-\xi^-$ are smaller than 10^{-3} fb. Hence, most of the successful scenarios in the Ma model the process $e^-e^- \to \xi^-\xi^-$ is difficult to be seen. In the AKS model, the cross section of $e^-e^- \to S^-S^-$ is large, and its value amounts to about 15 pb at $\sqrt{s} = 1$ TeV in the present scenario. Above the threshold, the magnitude of the cross sections are not sensitive to $\sqrt{s}$, so that even if $m_{S^\pm}$ would be at the TeV scale, we might be able to test it at future multi-TeV linear colliders, such as the Compact Linear Collider [25]. Because $B(S^\pm \to \eta^0 H^\pm) \simeq B(H^\pm \to \tau^\pm \nu) \simeq 100$ %, the signal should be $\tau^-\tau^-\nu\nu\eta\eta$ with almost the same rate as long as $m_{S^\pm} < m_{N_R^\alpha}$. The background mainly comes from $W^-W^-\nu_e\nu_e$, and the cross section is about 2.3 fb (22 fb) for $\sqrt{s} = 500$ GeV (1 TeV). The branching ratio for the leptonic decay of W bosons is 30%, so that the rate of the final state $\ell\ell'\nu\nu\nu\nu$ is at most 2 fb. Therefore, the signal in the AKS model and in the Zee-Babu model can be seen.

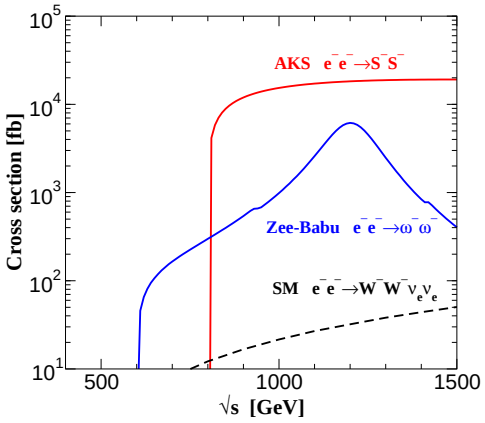

Figure 4: Cross sections of like-sign charged Higgs pair productions in the Zee-Babu model and in the AKS model.

There are several other models with lepton number violating interactions or right-handed Majorana neutrinos. Atwood et al. have discussed the signature of heavy Majorana neutrinos in the model without Z_2 symmetry via charged Higgs pair production at e^+e^- and e^-e^- collisions [26]. In supersymmetric models, Majorana particles also appear, and their effects also give similar t-channel contributions in the slepton pair production $e^-e^- \to \tilde{e}^-\tilde{e}^-$, whose cross section is at most $\mathcal{O}(100)$ fb. The final state would be $e^-e^-\chi^0\chi^0$ for example.

5 Conclusion

We have discussed general features of TeV-scale radiative seesaw models. They are characterized by an extended scalar (Higgs) sector and the Majorana nature. Various phenomenological aspects especially in experiments at the ILC. have been discussed in the Zee-Babu model (2-loop), the Ma model (1-loop), and the 3-loop model in Ref. [7]. While the extended Higgs sector can be explored at the LHC, the Majorana nature of the models can directly be tested at the ILC via the pair production of the charged scalar bosons at the electron-positron and electron-electron collision experiments.

References

[1] T. Yanagida, In Proceedings of Workshop on *the Unified Theory and the Baryon Number in the Universe*, p.95 KEK Tsukuba, Japan (1979); M. Gell-Mann, P. Ramond and R. Slansky, in Proceedings of Workshop *Supergravity*, p.315, Stony Brook, New York, 1979.

[2] A. Zee, Phys. Lett. B **93**, 389 (1980) [Erratum-ibid. B **95**, 461 (1980)]; Phys. Lett. B **161**, 141 (1985).

[3] E. Ma, Phys. Lett. B **662** (2008) 49; E. Ma, Mod. Phys. Lett. A **23** (2008) 721; R. A. Porto and A. Zee, Phys. Rev. D **79** (2009) 013003; E. Ma and D. Suematsu, Mod. Phys. Lett. A **24** (2009) 583; T. Hambye, K. Kannike, E. Ma and M. Raidal, Phys. Rev. D **75**, 095003 (2007).

[4] A. Zee, Nucl. Phys. B **264**, 99 (1986); K. S. Babu, Phys. Lett. B **203**, 132 (1988).

[5] L. M. Krauss, S. Nasri and M. Trodden, Phys. Rev. D **67**, 085002 (2003).

[6] E. Ma, Phys. Rev. D **73**, 077301 (2006).

[7] M. Aoki, S. Kanemura and O. Seto, Phys. Rev. Lett. **102**, 051805 (2009); Phys. Rev. D **80**, 033007 (2009).

[8] K. S. Babu and C. Macesanu, Phys. Rev. D **67**, 073010 (2003).

[9] D. Aristizabal Sierra and M. Hirsch, JHEP **0612**, 052 (2006).

[10] M. Nebot, J. F. Oliver, D. Palao and A. Santamaria, Phys. Rev. D **77**, 093013 (2008).

[11] N. G. Deshpande and E. Ma, Phys. Rev. D **18** (1978) 2574.

[12] Q. H. Cao, E. Ma and G. Rajasekaran, Phys. Rev. D **76** (2007) 095011.

[13] L. Lopez Honorez, E. Nezri, J. F. Oliver and M. H. G. Tytgat, JCAP **0702** (2007) 028.

[14] M. Aoki, S. Kanemura, K. Tsumura and K. Yagyu, Phys. Rev. D **80** (2009) 015017; S. Su and B. Thomas, Phys. Rev. D **79**, 095014 (2009); H. E. Logan and D. MacLennan, Phys. Rev. D **79**, 115022 (2009).

[15] A. Belyaev, R. Guedes, S. Moretti and R. Santos, arXiv:0912.2620 [hep-ph].

[16] M. Aoki and S. Kanemura, Phys. Lett. B **689**, 28 (2010).

[17] E. Lundström, M. Gustafsson, and J. Edsjö, Phys. Rev. D **79** (2009) 035013.

[18] J. Kubo, E. Ma and D. Suematsu, Phys. Lett. B **642**, 18 (2006); D. Aristizabal Sierra, J. Kubo, D. Restrepo, D. Suematsu and O. Zapata, Phys. Rev. D **79** (2009) 013011; D. Suematsu, T. Toma and T. Yoshida, Phys. Rev. D **79** (2009) 093004.

[19] V. D. Barger, J. L. Hewett and R. J. N. Phillips, Phys. Rev. D **41**, 3421 (1990); Y. Grossman, Nucl. Phys. B **426**, 355 (1994).

[20] M. Aoki, S. Kanemura and O. Seto, Phys. Lett. B **685**, 313 (2010).

[21] G. Aad *et al.* [The ATLAS Collaboration], arXiv:0901.0512 [hep-ex].

[22] Di Girolamo and B, Neukermans, L 2003 *Atlas Note* ATL-PHYS-2003-006; M. Warsinsky [ATLAS Collaboration], J. Phys. Conf. Ser. **110**, 072046 (2008).

[23] M. Schumacher, Repot No. LC-PHSM-2003-096.

[24] A. Pukhov *et al.*, arXiv:hep-ph/9908288. A. Pukhov, arXiv:hep-ph/0412191.

[25] E. Accomando *et al.* [CLIC Physics Working Group], arXiv:hep-ph/0412251.

[26] D. Atwood, S. Bar-Shalom and A. Soni, Phys. Rev. D **76** (2007) 033004.